IEEE Access
Multidisciplinary | Rapid Review | Open Access Journal

Received July 21, 2021, accepted August 16, 2021, date of publication August 20, 2021, date of current version August 30, 2021.

Digital Object Identifier 10.1109/ACCESS.2021.3106588

A Multi-Band Near Perfect Polarization and Angular Insensitive Metamaterial Absorber With a Simple Octagonal Resonator for Visible Wavelength

SULTAN MAHMUD[1], MINHAZUL KARIM[1], SIKDER SUNBEAM ISLAM[1], (Member, IEEE), MD MIZAN KABIR SHUVO[2], TANZINA AKTER[3], ALI F. ALMUTAIRI[4], (Senior Member, IEEE), AND MOHAMMAD TARIQUL ISLAM[5], (Senior Member, IEEE)

[1]Department of Electrical and Electronic Engineering, International Islamic University Chittagong, Chittagong 4318, Bangladesh
[2]Department of Electrical and Electronic Engineering, Mymensingh Engineering College, University of Dhaka, Dhaka 1000, Bangladesh
[3]Department of Chemistry, Government City College Chittagong, National University, Gazipur 1704, Bangladesh
[4]Electrical Engineering Department, Kuwait University, Kuwait City 13060, Kuwait
[5]Department of Electrical, Electronic and Systems Engineering, Faculty of Engineering and Built Environment, Universiti Kebangsaan Malaysia, Bangi, Selangor 43600, Malaysia

Corresponding authors: Sultan Mahmud (sultaniiuc3ni@gmail.com), Ali F. Almutairi (ali.almut@ku.edu.kw), and Mohammad Tariqul Islam (tariqul@ukm.edu.my)

ABSTRACT A multi-band, ultrathin, polarization-insensitive, near-perfect metamaterial absorber (PMA) has been proposed and substantiated numerically for solar thermophotovoltaic (STPV) systems which also can be used in some other applications. This kind of absorber currently drawing massive interest throughout the research of optics. Especially in solar harvesting metamaterial absorbers can give a huge boost in efficiency by intensifying the solar electromagnetic wave. Visible wavelength has been the key focus of the proposed design so that the structure can utilize solar energy proficiently. Aluminum (Al) and Gallium Arsenide (GaAs) have been chosen as materials for their higher electron mobility along with good temperature stability. The PMA is a three-layer metal-dielectric-metal called sandwiched structure. For proper characterization of the PMA absorber, extensive parametric inspections were carried out with underlying physics. The finite integration technique (FIT) in computer simulation technology microwave studio (CST MWS) is used to perform the numerical analysis and for verification finite element method (FEM) in COMSOL Multiphysics has been used along with interference theory model (ITM) for calculating the absorbance. The PMA shows 99.27%, 99.89%, 99.91%, and 99.06% perfect absorption at 454.75nm, 505.53nm, 568.72nm, and 600.85nm resonance wavelength in all three modes of waveguide propagation. The design also exhibits incident wave stability up to 60° for both transverse electric (TE), and transverse magnetic (TM) wave modes. Excellent glucose concentration sensing ability was also observed with the proposed structure. So, the proposed PMA can be implemented in solar energy harvesting devices along with solar sensors or detectors, light trappers, light modulators, or light wavelength detectors.

INDEX TERMS Metamaterial absorber, polarization-insensitive, STPV, visible wavelength, sensor.

I. INTRODUCTION

Metamaterial innovation is being used to address the issue of solar energy harvesting by designing more efficient absorbers in recent times [1]–[5]. Because such metamaterials have a variety of remarkable electromagnetic properties, metamaterial designs and applications have been a focus of intense study [6], [7]. Veselago theoretically examined the electrodynamic effects of a medium with both negative permittivity and permeability and concluded that the propagative properties of this medium are significantly different [8]. Smith *et al.* [9] found a feigned metamaterial with negative

The associate editor coordinating the review of this manuscript and approving it for publication was Raghvendra Kumar Chaudhary.

permeability and permittivity which shows double negative properties. Landy *et al.* identified different metamaterial absorbers (MA) which attracting a great deal of interest from researchers, including PMAs in the millimeter to millimeter range [10], [11], nanometer ranges [12], [13], multi-band [14], [15], and the ultra-large band [16]. Generally, a three-layered metal-dielectric-metal structure is supposed to be near PMA in solar wavelength. Metal layers prevent the propagation of the EM waves, and a coupling capacitance is constructed between the back-layer and the resonator in an MA with the help of a dielectric substance [17], [18]. Plasmonic resonance characteristics of a dielectric substrate [19], [20], perfect impedance match [21], [22], symmetric structure of the resonator [23], [24], and a good E-field, H-field and surface charge distribution [25], [26] causes high absorption of an PMA. Most common MA absorber structures are three-layered structures [27], [28], but there are also two-layered [29], four-layered [30], [31], multi-layered stacks [32]–[35]. Because of the periodic structure of PMAs, high absorption properties are exhibited over a large wavelength despite the PMAs being ultrathin [20], [36], [37], and polarization-insensitive [38], [39].

A. M. Montaser suggested an MA for all bands from microwave to Terahertz range and this absorber has 99.46% at 265.8THz and 99.4% at 556.4THz when the dimensions of the substrate are 2750 $\times$ 2750 nm^2 and 1150 $\times$ 1150 nm^2 respectively [40]. A metamaterial absorber unit cell structure with 500 $\times$ 500 nm^2 dimensions was recommended by Ustunsoy *et al.* which has a 99.99% absorptivity rate at 558.75THz and 99% absorptivity rate at 216.75THz [41]. For solar harvesting, Mulla *et al.* offered an MA which has an absorptivity rate of 98.2% at 445.85THz, and a peak of absorptivity of 99.4% in between 624THz and 658.3THz with Aluminum (Al) and Silicon Dioxide (SiO_2) three-layer structure [42]. An MA consists of TiN-SiO_2-TiN sandwiched structure shows an average absorption of 95% for the visible regime at TE and TM modes where TiN creates surface plasmonic component [43]. $Ge_2Sb_2Te_5$ (GST) used as a phase-change material along with gold for a new MA suggested by C. Tun *et al.* executed 96.8% and 96.2% absorptivity at 610nm and 870nm wavelength respectively [44]. Yu *et al.* offered a symmetric resonator (Ti/SiO_2) based MA with 500 $\times$ 500 nm^2 dimension which has absorption 96.67% at 538.9nm, 98.63% at 954.2nm, and 98.20% at 1726.5nm [45]. Zhang *et al.* discussed an MA (Al/SiO_2) with 370 $\times$ 370 nm^2 dimension which has above 95% absorption at 450nm and 584 nm wavelength at normal incidence [46]. An Au elliptical and circular disk array-based absorber that has three absorption peaks at 1.15μm, 1.55μm, and 2.05μm with an absorption rate of 99.2%, 99.7%, and 97.3% accordingly [47]. Hossain *et al.* also worked on an MA that has 99.74%, 99.23%, and 99.82% absorption rate at 245.03THz, 376.13 THz, and 502.1 THz having a dimension of 690.52 $\times$ 690.52 nm^2 [48]. A 600 $\times$ 600 nm^2 MA based on Au nano-cuboids array was proposed by Qin *et al.* that has three absorption peaks 96.8%, 99.6%, and 99.2% at 1115 nm, 1593 nm, and 2039 nm wavelength respectively [49]. Wang *et al.* proposed a Cu-SiO_2-Cu based PMA which has 60° incident angle stability, shows three absorption peaks of 87.1%, 99.9%, and 99.6% at 872.54nm, 1008.69nm and 1138.62nm respectively [50].

Considering the earlier literature review, our main target is to find peak absorbance above 99% at the visible regime range as it is important for solar harvesting, solar cells, or solar sensor, and other applications. A simple octagonal shape ultrathin nanostructured double negative (DNG) metamaterial absorber has been proposed from 400nm-700nm with four near-perfect absorptions endorsing Aluminum (optical) and Gallium Arsenide (loss-free) as metal and substrate. FIT is used to perform the numerical analysis of the absorbance and reflectance from scattering parameters in CST MWS software and the numerical analysis is verified with FEM in COMSOL Multiphysics software. Also, calculated absorption has been extracted by ITM. This design accomplishes four absorption peaks of 99.27%, 99.89%, 99.91%, 99.06% at 454.75 nm, 505.53 nm, 568.72 nm, and 600.85 nm respectively which all are situated in the visible regime. In all three propagation modes such as transverse electromagnetic (TEM), transverse electric (TE), and transverse magnetic (TM) mode the designed PMA shows almost similar absorbance and reflectance. This kind of good absorption peak is mostly due to a good impedance match with strong plasmonic resonance. The absorbance peak of our proposed configuration is superior to many other proposed metamaterials unit cells in [40], [51], [52], also will be discussed below. Industrially available materials were introduced in the proposed design so that it would be easy to produce the proposed PMA industrially. Due to the simple shape of the resonator, it will be easy to fabricate such a structure. The development of the proposed structure would open new scope of possibilities for more effective STPV solar cells. Also, this design can be easily implemented as a glucose concentration sensor applied an analyte layer over the unit cell. Moreover, this design also can be used in solar energy harvesting, solar sensor, light trapping, light modulator, or light detector. Technological advancement into these types of MAs would usher in a new era of industry-specific implementations.

II. DESIGN AND SIMULATION SETUP

A. CHOICE OF MATERIALS, UNIT CELL DESIGN, AND SIMULATION SETUP

The main inconvenience today is to approach the MA with materials such as good optical characteristics with high-temperature resistance. Although the broadband absorber with plasmonic materials is almost perfect, it is still operational. Metal and dielectric layers that are stable in high temperature and possess perfect optical properties have been chosen, because the proposed metamaterial structure operates in the optical wavelength. Metallic aluminum (Al)

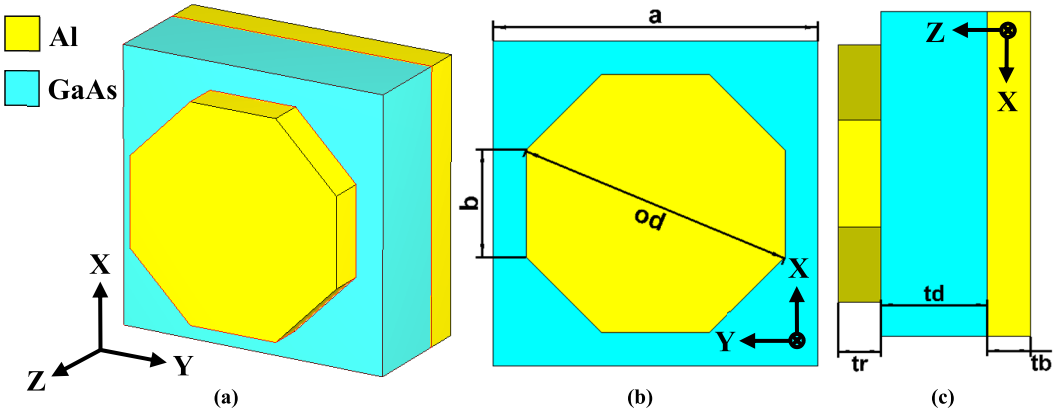

FIGURE 1. Design of the unit cell exhibited in (a) 3D view, (b) front view with physical dimension mentioned with parameters, and (c) side view along with axis.

TABLE 1. Parameter's list of proposed PMA structure.

Parameters	a	tb	td	tr	od	b
Value (nm)	566	75	260	75	487.06	186.39

with optical properties is among the most widely measured and analyzed optical properties of any material [53].

Gallium Arsenide (GaAs) which is a loss-free dielectric can be widely found in compound semiconductors, can absorb sunlight with a few microns of thickness [54]. Also, GaAs cells are in contrast to silicone cells comparatively heat and radiation-tolerant [55], [56].

Al (optical) and GaAs (loss-free) are suited best for this particular design. So, an Al-GaAs-Al three-layered sandwiched structure is harvested here shows in Fig. 1(a). However, the design and the thickness of the layers are very much crucial for controlling the efficiency of the cell. The proposed model substrate and back layer metal are square-shaped with the length of "a = 566nm" exhibit in Fig. 1(b). By using a square-shaped substrate and metal with different thicknesses, different results can be achieved with different significances. The best absorption rate is found at 566 × 566 nm^2 size and 410 nm thickness. Designing the Aluminum resonator is another crucial part of this modeling. It is known that when a material deals with a wavelength greater than its size it shows unusual characteristics and becomes metamaterial [9], [57]. The designed resonator has an octagonal shape and the length of the edge is "b = 186.39nm". Hence the resonator is designed in such a parameter that the visible wavelength is greater than its edge. Because of the octagonal shape, the resonator became polarization insensitive. The thickness of the resonator, dielectric substance, and back-layer has been chosen as "tr = 75nm", "td = 260nm", and "tb = 75nm" nm respectively and it also has a significant effect on the absorption rate can be seen from Fig. 1(c). Here, table 1 shows the parameter list of the proposed unit cell.

Here, for the TEM mode, periodic boundary conditions with a perfect electric conductor (PEC) and Perfect Magnetic Conductor (PMC) are applied in the x-axis and y-axis respectively. A waveguide port is initiated in the negative z-axis to pass the operating wavelength. Open space on both sides of the z-axis with a Perfectly Matched Layer (PML) is applied to reduce scattering. A linearly polarized planar wide-spectrum wave incidence on the top surface of the intended absorber. For TE and TM mode floquet port has been applied on the z-axis with a master on the x-axis and slave on the y-axis. The frequency-domain solver in the Computer Simulation Technology Microwave Studio (CST MWS) is used to simulate the model which runs the solver based on FIT. For numerical verification, FEM is used with COMSOL Multiphysics software. Floquet analysis can be done using a frequency-domain solver. Frequency domain solvers are useful for smaller structures like unit cells and FSS (Frequency Selective Surface). Based on the transient behavior of the source of excitation and modes, frequency domain solvers often require less time and memory than other solvers.

III. RESULTS ANALYSIS AND DISCUSSION

A. METHODOLOGY

The scattering parameters of (1) and (2) (S-parameter) are derived from the procedure of Nicolson–Ross–Weir (NRW) as described in the reference for the measurement of absorbance [58]. Impedance match is highly desirable for measuring absorption. For IR and visible wavelength, the optical properties of Aluminum and Gallium Arsenide are available in acquired from (3) and (4) [59]. An Electromagnetic wave incident is replicated and transferred to a metamaterial substrate. By limiting $R(\omega) = |S_{11}|$ and $S(\omega) = |S_{21}|$, high absorbance can be obtained,

$$S_{11} = S_{22} = \frac{i}{2}\left(\frac{1}{z} - Z\right) sin\,(nkd) \tag{1}$$

$$S_{21} = S_{12} = \frac{1}{cos\,(nkd) - \frac{i}{z}\left(Z + \frac{1}{2}\right) sin\,(nkd)} \tag{2}$$

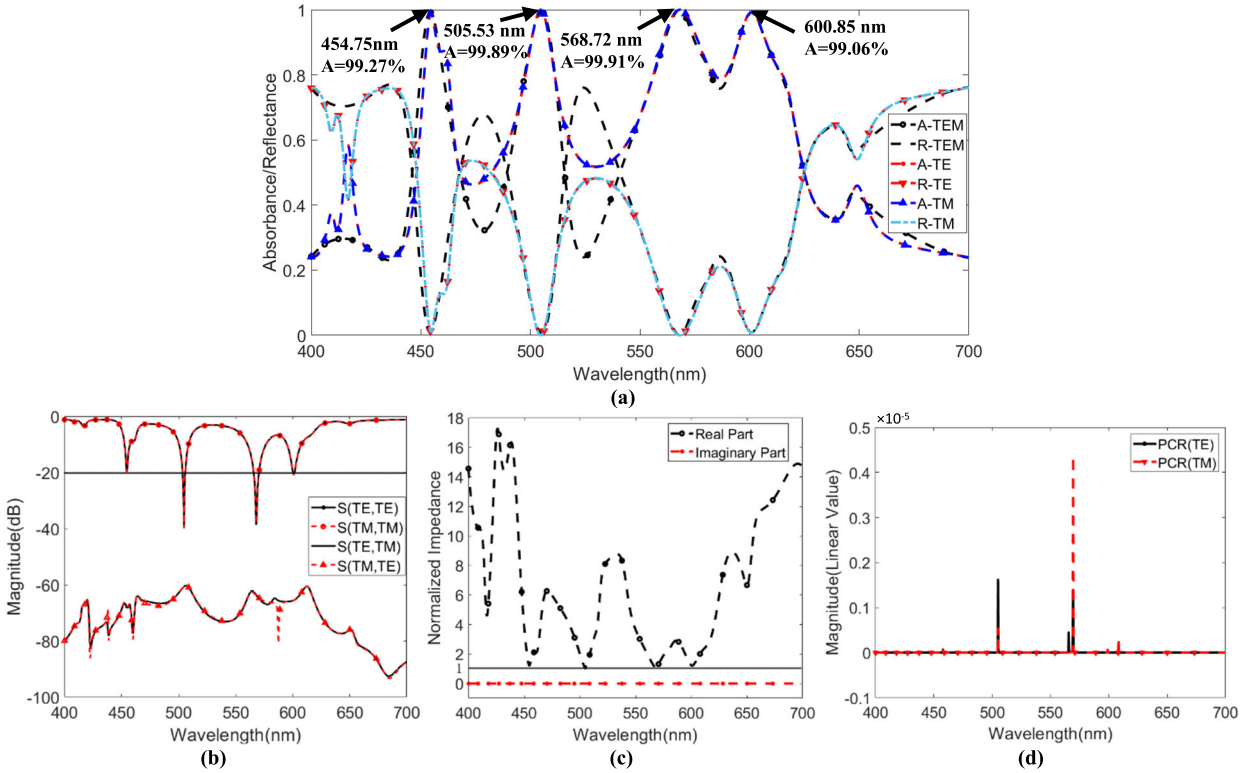

FIGURE 2. Graphical representation of (a) TEM, TE, and TM mode absorbance and reflectance, (b) magnitude (dB) value of co and cross-polarization components of the proposed structure in TE and TM modes, (c) normalized impedance in real and imaginary parts in linear value, and (d) magnitude (linear value) polarization conversion ratio (PCR) in TE and TM modes for 400nm-700nm range.

Here,
S_{11}, S_{22}, S_{21}, and S_{12} are S parameters,
n = Effective Refractive Index,
k = Wave Vector,
d = Thickness of the designed structure.
The impedance of the unit cell,

$$Z = \pm\sqrt{\frac{(1+S_{11})^2 - S_{21}^2}{(1-S_{11})^2 - S_{21}^2}} \tag{3}$$

$$Z(\omega) = \left[\frac{\mu_r(\omega).\mu_0}{\varepsilon_r(\omega).\varepsilon_0}\right]^2 \tag{4}$$

and characteristic impedance $Z_0 = (\mu_0/\varepsilon_r)^{1/2} = 376.73 \approx 377\Omega$. Here,
μ_0 = Permeability of Free Space,
ε_0 = Permittivity of Free Space,
μ_r = Relative Permeability and
ε_r = Relative Permittivity.

Condition ($Z(\omega) = Z_0$) can be obtained by changing the physical dimensions of the design step by step. However, If $Z(\omega) = Z_0$ can be gained, the design will become a super absorber with unity absorption. So, in every MA $Z(\omega)$ is slightly lesser than Z_0 in practical design. The scattering parameters (S_{11} and S_{21}) of an MA are inversely proportional to absorbance. Absorption can be measured from (5),

$$\begin{aligned} A(\omega) &= 1 - R(\omega) - T(\omega) \\ &= 1 - |S_{11}(\omega)|^2 - |S_{21}(\omega)|^2 \end{aligned} \tag{5}$$

Here,
$R(\omega) = S_{11}$, reflection coefficient, and
$T(\omega) = S_{21}$, transmission coefficient.

However, transmission coefficient $T(\omega)$ is near zero, because the thickness of aluminum of design blocks all EM waves as the ground-layer thickness was higher than the skin depth (δ) $= (2\rho/2\pi f\mu R\mu_0)^{1/2}$. So, final absorption can be emulated from (6),

$$A(\omega) = 1 - R(\omega) = 1 - |S_{11}(\omega)|^2 \tag{6}$$

B. ABSORPTION CHARACTERISTICS

Fig. 2(a) shows the properties of absorption by using metal and resonating material as an aluminum (optical) and dielectric substrate as Gallium Arsenide (loss-free), for TE, TM and TEM modes. The s-parameter from the simulation calculates these results. The absorption in all three modes is excellent from 400nm- 700nm with four absorption peaks of 99.27% (peak-1) at 454.75 nm, 99.89% (peak-2) at 505.53 nm, 99.91% (peak-2) at 568.72 nm, and 99.06% (peak-4) at 600.85 nm. The TE and TM modes are nearly identical in terms of absorption, with all absorption levels above 99%, since the design is very much symmetrical. The structure has almost the same absorption in the TE and TM modes compared with TEM mode, with near-unity absorption of all four peaks above 99%. Fig. 2(b) shows that the design - exhibits an s-parameter up to −20 dB at the same wavelength where the peak absorptions were obtained. This is one of

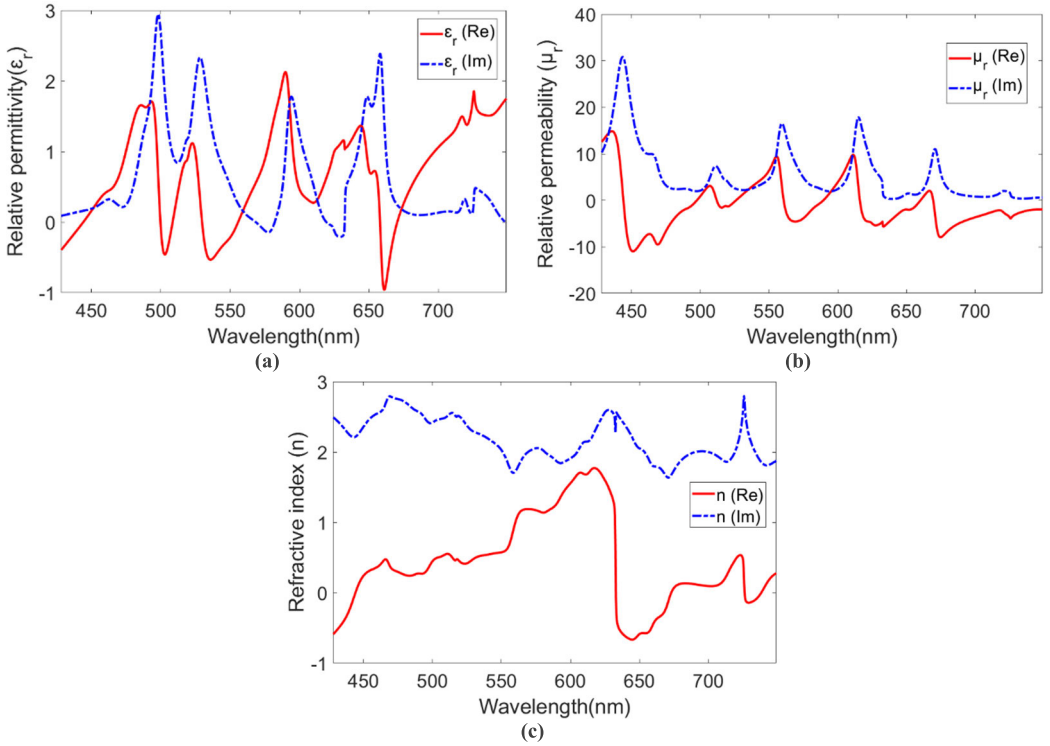

FIGURE 3. Simulated analysis of the proposed PMA for metamaterial characteristics such as (a) real and imaginary parts of the relative permittivity (ε_r), (b) real and imaginary parts of relative permeability (μ_r), and (c) real and imaginary parts of refractive index (n).

the reasons why the design got four near unity absorptions. Since the unit cell is designed with aluminum, resonator, and ground-layer to create an excellent impedance match with free space, aluminum surface plasmons do not operate in the visible region [60]. The inherent loss of the resonator is another explanation for the high impedance match. With the thickness of 260 nm, gallium arsenide reduces the gap from the resonator to the ground layer, creating plasmonic resonance characteristics. It is known that the real parts of the normalized impedance should be near unity for a high impedance match, where the imaginary parts should stay near zero. This matter can be exhibit in Fig. 2(c). Very good capacitive and inductive coupling of metal and dielectric resonator layer is also an important phenomenon for good absorption in the whole visible region. The electromagnetic wave is imprisoned by the symmetrically shaped resonator, which recollects the wave with complex dispersion and is confined to a dielectric layer. The symmetricity of the design can be easily understood by Fig. 2(d), as it is seen that the polarization conversion ratio (PCR) of this proposed structure is near zero over the full optical range. This also ensures that the MA is a perfect absorber rather than a polarization converter.

C. EXTRACTING METAMATERIAL PROPERTIES OF THE PROPOSED PMA

The EM properties of a PMA such as relative permittivity, relative permeability, the refractive index (RI) can be extricated from the NRW equation [58], [61], [62] as depicts in Fig. 3. After extracting the reflection-coefficient (S_{11}) and transmission-coefficient (S_{21}) from CST MWS simulation software as given in (1) and (2), those values can be used for further calculation of NRW. From (7), S_{21} can be expressed as (7) where $s_0 = \pm 1$ and $M = (1 - |S_{11}|^2/1 - |S_{11}|^2)^{1/2}$. Also, the magnitude (dB) of S_{11} remains the same but s_0 polarity is changed from $-\pi$ to $+\pi$ with the EM wave. A multi-band PMA always provides fluctuating point as shown in Fig. 3.

$$S_{21} = js_0 S_{11} M \tag{7}$$

In free space, perpendicular and parallel polarization in TE or TM mode shows a relationship with the square of the wave vector k and susceptibility κ of the normal incident. Here $k = 2\pi f/c$, where, c is the speed of light and f is denoted as frequency. It is known that dielectric losses are correlated to the imaginary part of the relative permittivity (ε_r) and polarization degree represents by the real part. In Fig. 3(a), good relative permittivity (ε_r) is guided by the high polarization value. Also, the dielectric spacer constant was opposite of the polarization value, but this consequence is neglected due to an excessive change in the field. Energy absorption is correlated with the positive part of an imaginary value, which depends on the capacitor charge between the metal plane and resonator along with the dielectric placer. Again, excessive change in EM field in high wavelength, majority materials behave like plasma - oscillator. From Fig. 3(a)-(c), it can be easily understandable that real parts should stay

in positive portion and approach to one, where imaginary parts should approach zero. This phenomenon has also been reported in many works previously reported [63]–[66]. Also, the near-zero values of the real parts of the relative permeability (μ_r), exhibit the spatial dispersion in resonance wavelength. Moreover, the negative dispersion with a non-physical part has a definable value. By the direct refractive index (DRI) method another important characteristic of a PMA can be extracted which is refractive index (n). A negative RI is expected as per as (10) and (11) discussed below. Conjugated to the relative permittivity and permeability, real parts of the RI should have negative in some specific ranges. From Fig. 3, it can be seen that in this specific design, there was a negative RI along with negative permittivity and permeability. So, the design can be characterized as a double negative (DNG) metamaterial absorber. This section also clarifies that why the specific design finds four bands in the visible range.

D. COMPARATIVE ANALYSIS WITH DIFFERENT METALS AND SUBSTRATES LAYERS

Fig. 4 shows some comparative analysis of different metals and substrates for understanding the absorption properties. Here, Fig. 4(a) demonstrates metal sweep analysis among Tungsten, Iron, Copper, and Silver for the proposed design along with Aluminum. From there, it is seen that Tungsten shows wide-band absorption but absorption is not good, it shows above 90% absorption only once. When Copper is used as a metal, it shows only one absorption of 95.47% at 643.97 nm. Similarly, Silver exhibits bad absorptions for the design and has only one absorption peak of 99.01% at 680.60 nm. So, it is proved that W and Cu did not match the desired impedance for the structure. When Silver is replaced by Iron, the design is exposed by four good absorption peaks 455.22 nm, 483.26 nm, 541.9 nm, and 577.79 nm are 99.61%, 99.12%, 95.12%, and 99.55%. But when we implement Al as metal, we get better absorption than Silver. aluminum shows four absorption peaks and all of them are above 99%, where Silver shows three peaks above 99%. Thus, Aluminum is perfect for metal selection with good absorption and desired impedance match in those four peak bands.

The comparative absorbances for several substrates are demonstrated in Fig. 4(b). The Figure shows absorbance for GaAs, Zinc Oxide, Silicon dioxide, Silicon nitrite, and FR-4. When GaAs are applied as substrate, the design exhibits four finest absorptions at 454.75 nm, 505.53 nm, 568.72 nm, and 600.85 nm are 99.27%, 99.89%, 99.91%, and 99.06% respectively. Here it is seen that all four peaks are above 99% and there is no distortion in these peaks. When GaAs are replaced with ZnO, the structure shows five absorptions at 463.34 nm, 474.65 nm, 524.24 nm, 563.15 nm, and 700 nm are 99.57%, 94.14%, 99.8%, 91.21%, and 98.06%, respectively. But it is seen that among the peaks only two are above 99%. For SiO_2 substrate, the design shows only three absorption peaks above 99%. Similarly, SiN shows only one absorption above 99% and FR-4 has no absorption above 99%. So, it can be seen that GaAs exhibit four absorption peaks, and all of them are above 99%. Therefore, due to its high absorption peaks, GaAs are considered the optimum dielectric substrate material for the proposed design.

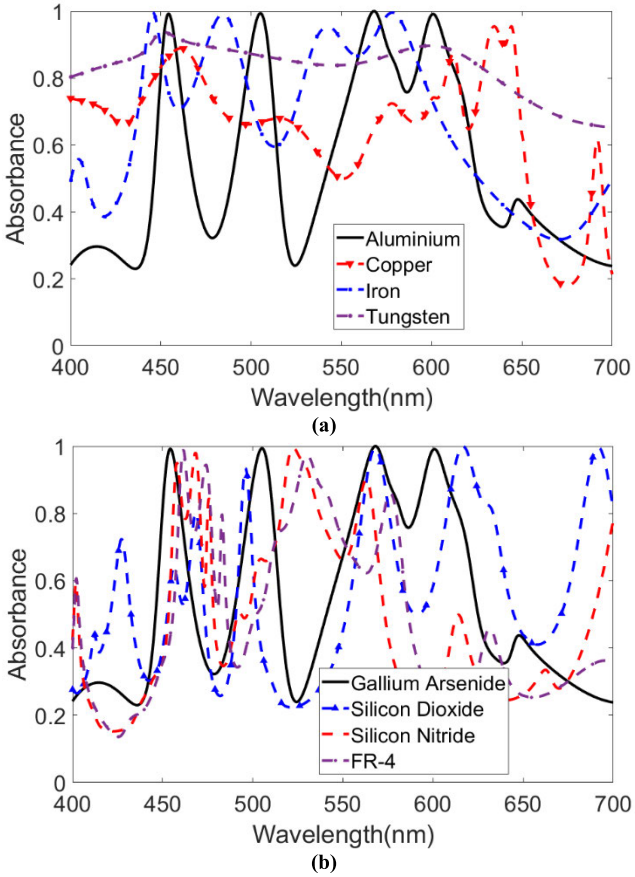

FIGURE 4. Comparison of absorption with (a) different metal and (b) dielectric layers.

E. POLARIZATION AND INCIDENT ANGLE STABILITY

For both TE and TM modes, it is mentioned above that the design is polarization and incident angle insensitive. A PMA must exhibit stable absorptivity for a high incidence angle to cast off as a solar energy harvesting device or many other important applications. For any four-fold symmetric structure of resonator, TE and TM polarization stability shows insensitive nature. As the proposed structure is four-fold symmetrical so, in this section we only discussed about the incident angular stability of the proposed structure.

Fig. 5(a) and Fig 5(b) demonstrates different absorption for different incident angles from 0° to 60° with an increment of 10° for both TE and TM modes. At 0° incident angle, the design shows four absorption peaks above 99% and after increasing incident angle from 10° to 60°, the absorption reduces gradually. But from Fig. 5(a) and Fig. 5(b), it is seen that the absorption peaks show 70% incident angle stability. The higher the incident angle, the higher the path distance.

That's why a wider electric field for the perpendicular incident angle is the explanation for better stability than

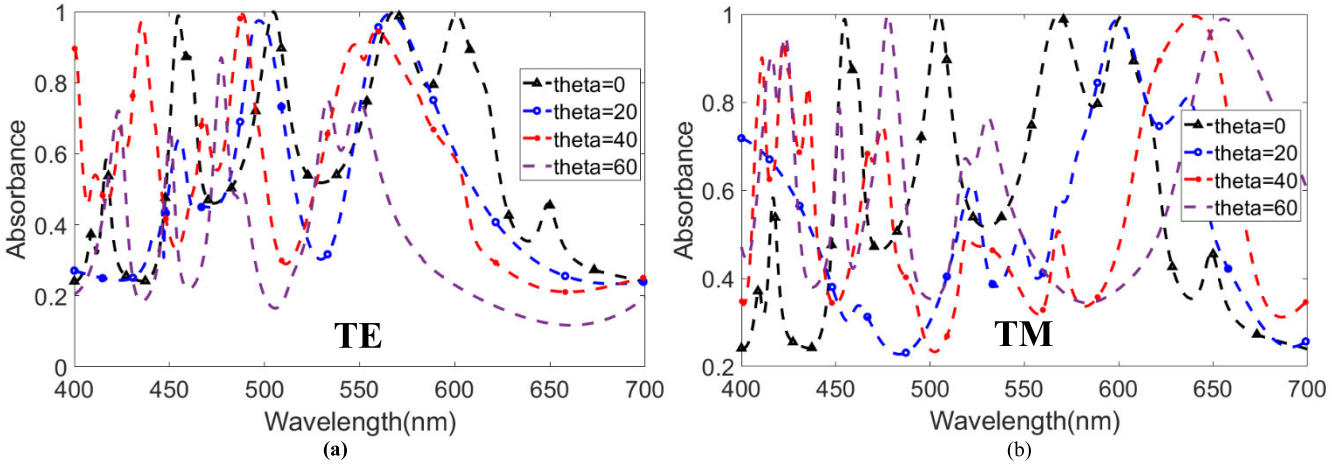

FIGURE 5. Representation of absorption characteristics for (a) different incident angles in TE mode, and (b) different incident angles in TM mode.

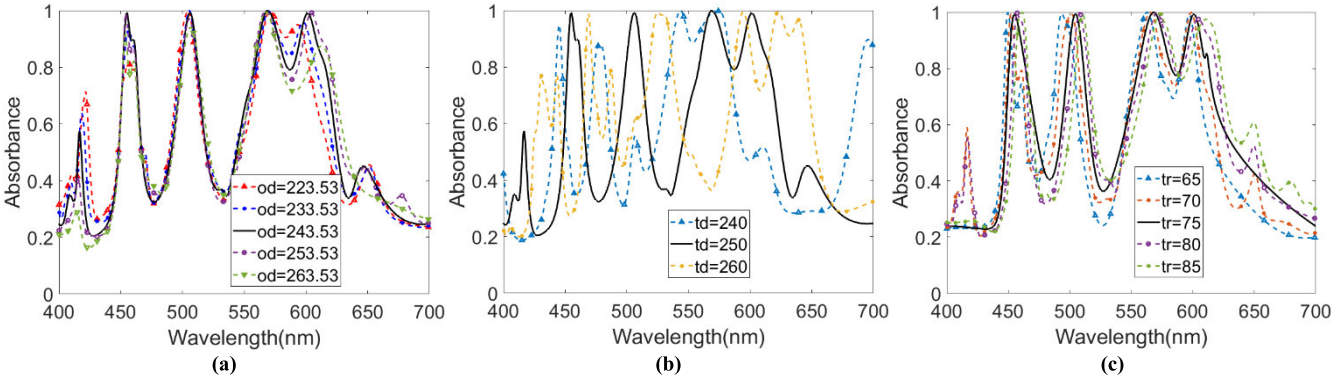

FIGURE 6. Parametric analysis of the proposed unit cell with (a) parameter "od = octagonal diameter", (b) parameter "td = dielectric thickness", (c) parameter "tr = resonator thickness."

the parallel element. However, this proposed design has an excellent coupling with a strong wave containment with a wide and polarized angle that enhances the implementation requirements to several fields as a robust MA.

F. GEOMETRIC PARAMETER ANALYSIS

The important parametric sweeps of the structure are demonstrated in Fig. 6. This parametric sweep helps to determine the highest absorbance peaks of the design. From Table 1, six parameters have been seen for this particular design. However, most three significant parameter sweeps have been demonstrated here. They are, the outer diameter of the octagonal resonator (od), the thickness of the dielectric substrate (td), and the thickness of the resonator (tr).

The parameter of structure od = 243.53 nm, td = 260 nm and tr = 75 nm. For these parameters, the structure achieved four best absorption peaks of 99.27% at 454.7567 nm, 99.89% at 505.5335 nm, 99.91% at 568.7259 nm, and 99.06 at 600.8599 nm. The absorption at other parameters is not good as these parameters. The parametric sweep was taken from 400 nm to 700 nm for the visible optical range.

When a plane wave is proliferating, two waves ruptured, which are transmitted waves and reflected waves subject to incidence angle and interruption of dielectric substance. However, incidence angle may result from extended wave components. As the PMA model highly depends on the dielectric parameters, the first parametric sweep was taken for outer diameter 'od'. By changing this parameter, from 223.53 nm to 263.53 nm with an interval of 10 nm, and the results showed in Fig. 6(a). From there, it is proved that od = 243.53 nm shows the best absorption because this parameter is suited best for an octagonal-shaped resonator on the dielectric layer. When the resonator was fitted to the substrate and metal, four absorption peaks were observed that were over 99%. Good inductive and capacitive coupling with resonator and back layer and perfect impedance match with the free space is the main reason for this kind of higher absorbance.

The second parametric sweep was taken for dielectric thickness 'td'. The sweep of the parameter 'td' showed a significant change. This sweep was taken by changing the value of td from 240 nm to 280 nm with an increment of 10 nm, and the results showed in Fig. 6(b). From that, it can be seen that reducing dielectric thickness, reduces the number of peaks and absorption rate. After increasing the 'td', the design exhibits more absorption peaks but these

peaks are getting distorted which is not desirable. But at td = 260 nm, the design exhibits four smooth and highest peaks absorptions which is the desired result. The mutual inductance increases as the value of 'td' are increased, but the self-inductance, which is generated by the metal and the resonator layer, decreases is the main cause for this kind of phenomenon.

The third parametric sweep was taken for resonator thickness by changing the parameter 'tr' from 65 nm - 85 nm with an increment of 10 nm, and Fig. 6(c) demonstrates the results. The design exhibits almost the same result at all 'tr' parameters, except tr = 70 nm and 80 nm have some small peaks before and after of four major peaks, which are less significant. But among all of the parameters, the design got all four major peaks above 99% when tr = 75 nm. That's why resonator thickness 75 nm is desirable for the design. The capacitance and inductance are proportional to the thickness of the resonator and metal. That's why absorption peaks have been shifted from left to right rather than higher or lower absorption values.

G. ELECTRIC FIELDS, MAGNETIC FIELDS, AND SURFACE CURRENT DENSITY

Without considering the traditional EM field equation, the electric field and magnetic fields can be described as (8) and (9) given below.

$$B_{avg} = \mu_{eff}\mu_0 H_{avg} \tag{8}$$

$$D_{avg} = \varepsilon_{eff}\varepsilon_0 E_{avg} \tag{9}$$

Here, B_{avg} is the average flux-density of the magnetic component, μ_{eff} is effective permeability, μ_0 is the permeability of the free space, H_{avg} is the average field-density of magnetic component, D_{avg} is the average flux-density of the electric component, ε_{eff} is effective permittivity, ε_0 is the permittivity of the free space, E_{avg} is average field density of electric component. Considering those equations, the integral form of maxwell's equation can be written as (10) and (11),

$$\int_C H.dI = 0 + \frac{d}{dt}\iint_S D.dS \tag{10}$$

$$\int_C E.dI = 0 - \frac{d}{dt}\iint_S B.dS \tag{11}$$

Here, H is magnetic field density and E denote electric field density respectively, and B is magnetic flux density and D magnetic electric flux density. With the nonuniform deviation of the magnetic field, the above equations can be calculated with the surface of the proposed model along with an instantaneously changed EM wave propagation. However, high absorption properties distinctly depend on EM field and surface current density for both TE and TM modes. Mostly, homogeneous field distribution, permittivity stays near unity, but for PMA magnetic flux and field is not the same because both of them, are inhomogeneous and asymmetric along with the EM wave. This results in an altered effective permeability. In a PMA a dielectric resonance is generated by the magnetic dipolar moment- between the resonator and the ground layer. Therefore, the absorption is primarily limited to GaAs, and for this effect the wavelength of the strong absorption increases. All of these matters are discussed separately in this section with Fig. 7 – 9. For deeper comprehension, six wavelength points with six levels of absorptivity are demonstrated here. They are $\lambda = 433.31$ nm, which has low absorptivity of 24.3%, peak bands, $\lambda = 600.85$ nm, 454.75 nm, 505.53 nm and 568.72 nm which have the highest absorptivity above 99%, and $\lambda = 624.86$ nm which has relatively medium absorptivity of 50.76%, for both TE and TM mode in normal incidence angle.

Fig. 7 exhibits E-field for both TE and TM polarization with six distinct wavelengths. This is one of the main reasons for the previously discussed higher absorption. In the center of the structure, the electrical field is primarily dispersed. High points of the e-field are primarily observed on the metal resonator/dielectric surface, which indicates the growing plasmon effect of the surface shown in Fig. 7(a)–7(f). These plasmons on the surface provided the ideal dipole for the magnification of the located E-field. The interfaces between aluminum and GaAs increase the surface plasmon in the MA which led it to high absorption in some particular points [17], [67]. The electrical dipolar resonance moment is stimulated by the e-field which is strongly confined in the dielectric substance GaAs layer evident in Fig. 7(m), Fig. 7(n), and Fig. 7(o) for both polarizations.

Fig. 8 demonstrated H-field for six wavelength points in both TE and TM polarization as like as E-field discussed above. As stable and disperse e-field, the proposed design shows a well-disseminated h-field for all four peaks shows in Fig. 8(a)–8(l). The h-field is highly located on the resonator and widely confined by the dielectric substance of the structure. For the four peak absorption levels, the h-field is very intensive for both TE and TM modes. Fig. 8(m), 8(n), and 8(o) show the intensity of the h-field in the dielectric layer. Here, at 568.72nm wavelength, the design exhibits a strong h-field in the center of the dielectric as it is the peak absorption point. The h-field changes direction only when the polarization mode is changed from TE to TM modes. A Loop from the back-layer to resonator produces a loop against parallel current density. The current density that is closely connected with the h-field increases the artificial magnetic dipolar moment [68]. The arrangement then excites the h-field and hints at a very powerful magnetic resonant dipole and produces an excellent absorption in the entire optical region.

As four-band resonance is resulted with the proposed PMA depict in the previous discussion after EM wave infiltrated, domination in propagation is not situated with either E-field or H-field mostly. Also, the domination of inductance and capacitance in the nock of the model creates a surface current density which proves a strong electric field. Also, in the four bands, the model shows a uniform magnetic field as it is supposed to be.

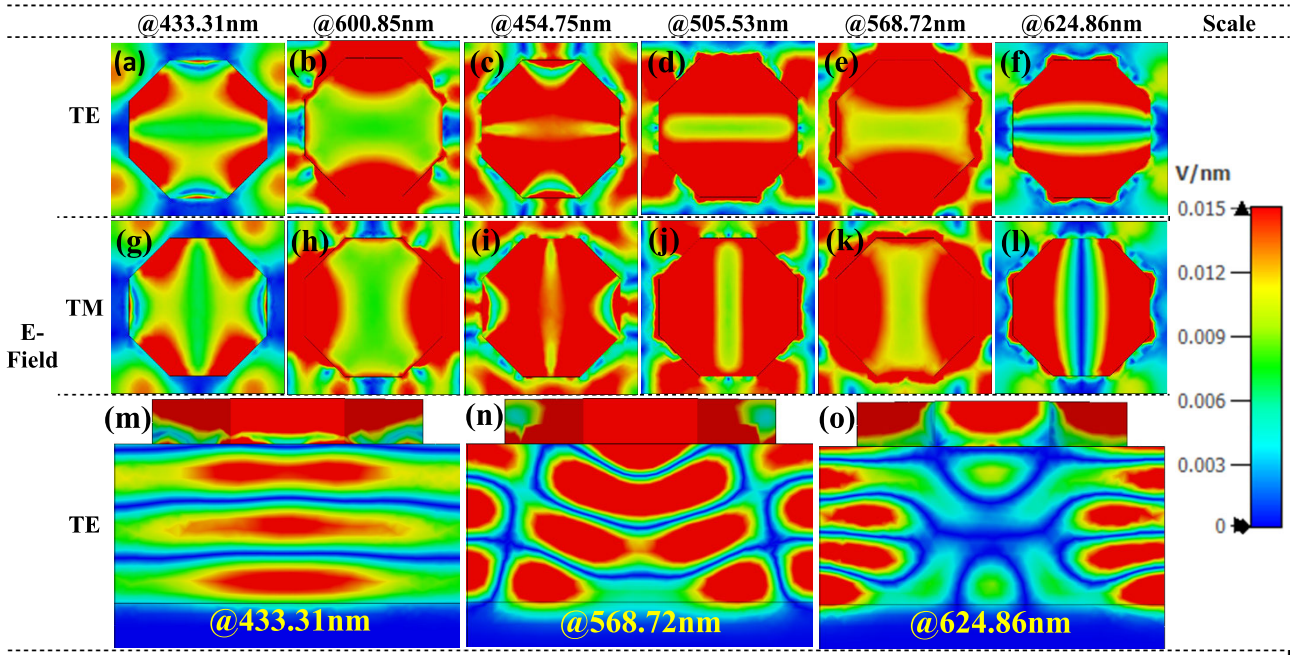

FIGURE 7. Representation of E-field contour map extracted from CST MWS (a)-(f) for TE mode at 433.31nm (low absorption point), 600.85nm (peak-1), 454.75nm (peak-2), 505.53nm (peak-3), 568.72nm (peak-4), and 624.86nm (mid absorption point) in y-x axis, (g)-(l) for TM mode at same points in y-x axis, and (m)-(o) cross-sectional view at 433.31nm, 568.72nm (peak-4), and 624.86nm respectively in z-y axis with linear color bar (Vnm^{-1}) for normal incidence angle.

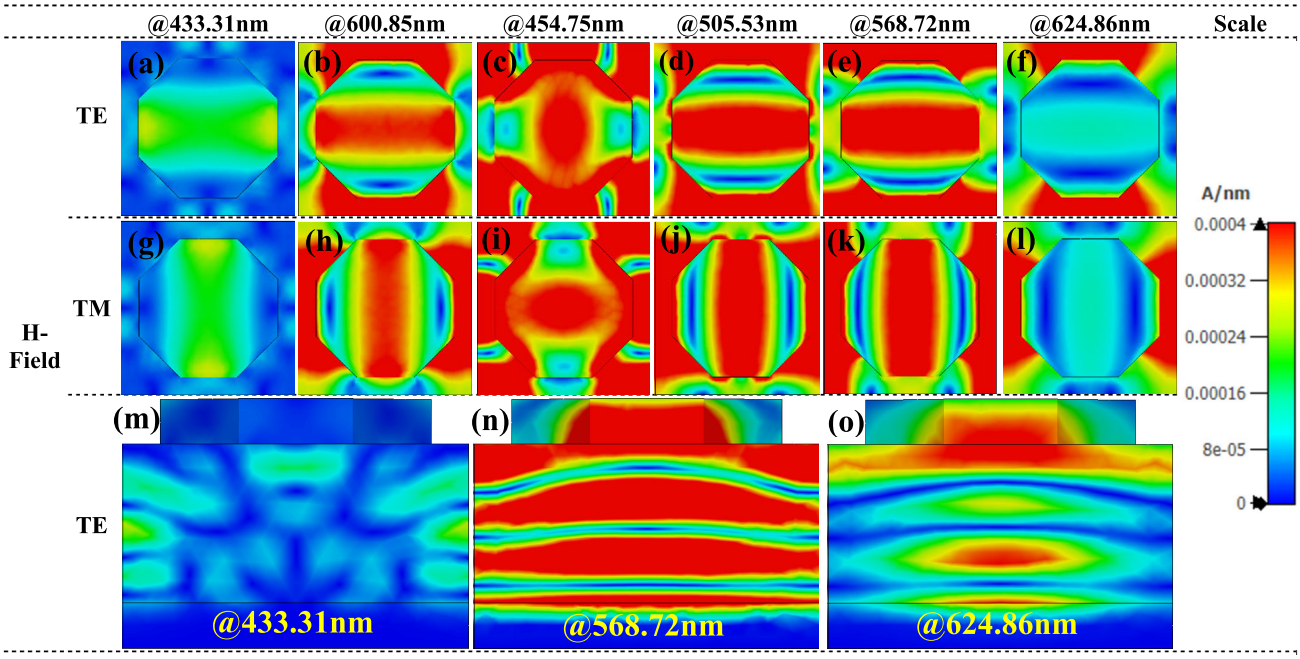

FIGURE 8. Representation of H-field contour map extracted from CST MWS (a)-(f) for TE mode at 433.31nm (low absorption point), 600.85nm (peak-1), 454.75nm (peak-2), 505.53nm (peak-3), 568.72nm (peak-4), and 624.86nm (mid absorption point) in y-x axis, (g)-(l) for TM mode at same points in y-x axis, and (m)-(o) cross-sectional view at 433.31nm, 568.72nm (peak-4), and 624.86nm respectively in z-y axis with linear color bar (Anm^{-1}) for normal incidence angle.

Helmholtz's equation affirms that less consumption of magnetic field happened when a homogenous field in a bi-anisotropic resonator emitted. Moreover, mutual coupling of resonator and ground plane receives the field in the center of the PMA, results in a prompted orientation of H-field. Surface current density is demonstrated in Fig. 9(a)–9(f) and Fig. 9(g)–9(l) for both TE and TM modes respectively. The figure shows that the surface charge is widely scattered

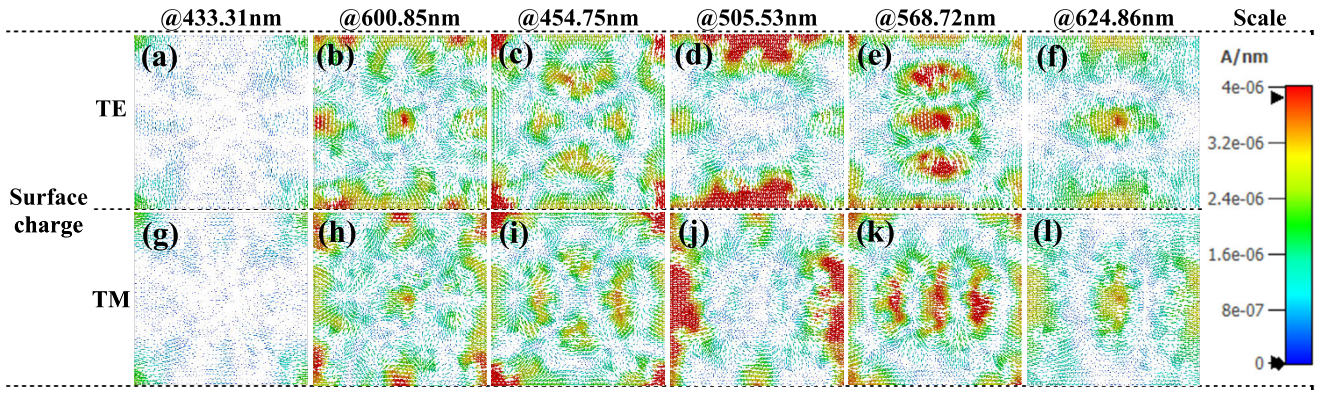

FIGURE 9. Representation of surface charge distribution in vector map extracted from CST MWS (a)-(f) for TE mode at 433.31nm (low absorption point), 600.85nm (peak-1), 454.75nm (peak-2), 505.53nm (peak-3), 568.72nm (peak-4), and 624.86nm (mid absorption point) in y-x axis, and (g)-(l) for TM mode at same points in y-x axis with linear color bar (Anm^{-1}) for normal incidence angle.

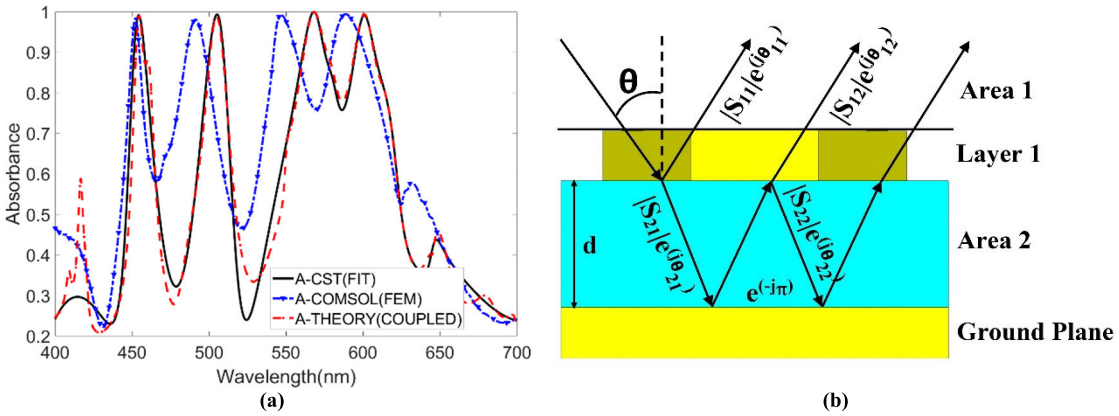

FIGURE 10. Demonstration of (a) absorbance phenomenon with CST MWS which works with the FIT, COMSOL Multiphysics simulation software which works with FEM and calculated absorbance using interference theory model, and (b) exhibition of interference theory model with different incidence angle theta.

over the entire cell unit at $\lambda = 600.85$ nm, 454.32 nm, 595.23 nm, and 567.95 nm. However, at $\lambda = 433.31$ nm and $\lambda = 624.86$ nm, the structure has less distribution than at $\lambda = 600.85$ nm, 454.32 nm, 595.23 nm, and 567.95 nm. From Fig. 9(a)-(l), it can be easily seen that the current on the resonator is asymmetric, which is also confirmed by the reflection coefficient (S_{11}). As a result, the model's surface current loop is created by the corresponding magnetic dipolar moment, which is responsible for the incorporating magnetic field of the proposed model. Finally, it can be said that the uniform distribution of the circulating surface charge is the cause of the strong electromagnetic field produced by the structure described above in the dielectric layer [69].

H. VERIFICATION OF NUMERICAL ANALYSIS IN A SIMULATION SOFTWARE AND WITH INTERFERENCE THEORY MODEL

In this approach, the design has been gone through under two different simulation software for numerical analysis and with interference theory model for calculated analysis showed in Fig. 10. Here, COMSOL Multiphysics which evaluates the numerical result with finite element method (FEM) has been comprehended in TEM mode. These two numerical analyses execute almost similar results with four near-perfect absorptions above 99%. However, little dissimilarity in absorption points has been glimpsed due to the divergence in materials properties in those two simulations. Finally, for more specific verification, the proposed PMA is measured with the interference theory model [70]–[75] also in TEM mode. From interference decoupled theory, $S_{11total}$ can be calculated by (12),

$$S_{11total} = |S_{11}|e^{j\theta}{}_{11} + ((|S_{12}||S_{21}|e^{j(\theta_{12}+\theta_{21}-2\beta-\pi)})/ \times (1 - |S_{22}|e^{j(\theta_{22}-\theta_{22}-2\beta-\pi)})) \quad (12)$$

Here, $S11 = |S_{11}|e^{j\theta}{}_{11}$, $S_{21} = |S_{21}|e^{j\theta}{}_{21}$, $S_{12} = |S_{12}|e^{j\theta}{}_{12}$, $S_{22} = |S_{22}|e^{j\theta}{}_{22}$ all of them represents the reflection coefficient from surface 1 show in Fig. 10(b). And, $\beta = kd$, where, β = circularize phase, k= wave number and d = dielectric spacer length. For the symmetrical shape, S_{12} can be replaced with S_{21}, and (12) can be rewrite as (13),

$$S_{11total} = |S_{11}|e^{j\theta}{}_{11} + ((|S_{12}|^{2ej(2\theta_{12}-2\beta-\pi)})/ \times (1 - |S_{22}|ej^{(\theta_{22}-2\beta-\pi)})) \quad (13)$$

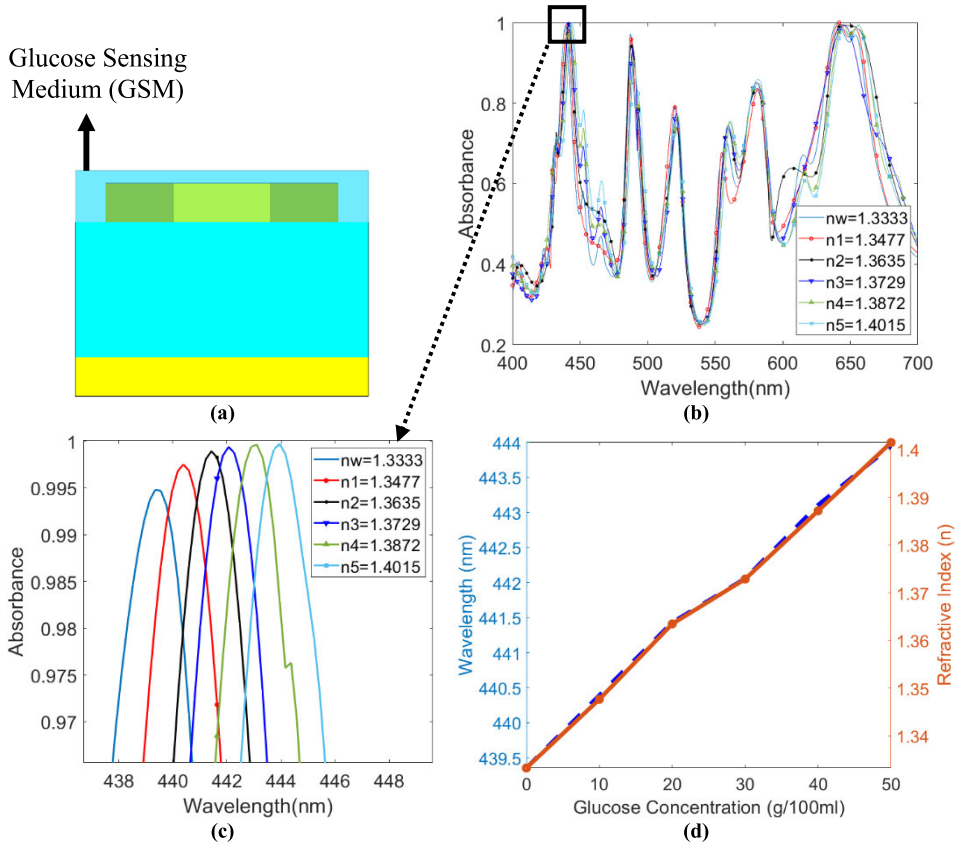

FIGURE 11. (a) Visual representation of the glucose-sensing medium, (b) graphical representation of absorption with different refractive index (n) of glucose concentration, (c) zoomed view of the selective absorption peak for sensing or detecting, and (d) glucose concentration versus wavelength graph (left) with glucose concentration versus refractive index graph (right).

And, the final absorption can be written as (14), which is plotted in Fig. 10(a).

$$A(\omega) = 1 - |S_{11total}|^2 \tag{14}$$

The figure verified that the numerically simulated absorption is close to the calculated absorption value which has been extracted from the interference theory model.

I. GLUCOSE CONCENTRATION SENSING PROPER-TIES OF THE PROPOSED METAMATERIAL ABSORBER

In this part, the response of the proposed MA with different glucose concentrations will be exhibited from 0 g/100ml to 50 g/100ml. Here, a glucose-sensing medium (GSM) has been grasped above the dielectric layer as the surrounding environment is shown in Fig. 11(a). The GSM layer refractive index (n) sets from the refractometric method depending on the concentration of glucose in water [76]. From the formula, $n = n_w + aC$ refractive index of glucose concentration can be determined. Here, n_w is the refractive index of normal water, $a = 0.00143$ is a fixed number, and C is the glucose concentration in g/100 ml. From this formula, the RI of the aqueous glucose solution has been determined. Here, $n_w = 1.3333$ as it stands RI of water, n_1, n_2, n_3, n_4, n_5, represents the RI of the aqueous solution of glucose in water for 10%, 20%, 30%, 40%, 50% in g/ 100 ml respectively. Then, simulated with the numerical method to see the response of the proposed MA. A successive increment of the RI increases the effective capacitance of the proposed MA, which results in shifts of the resonance wavelength [77]–[80]. Fig. 11(b), demonstrated the absorption phenomenon of the design with GSM for the full visible region. Fig. 11(c) shows that the resonance wavelength increased as the value of the RI increases. At last, Fig. 11(d) ensures that the resonance wavelength increases linearly with glucose concentration with water. Thus, with the swap of the RI value of the surrounding GSM environment, shifts of the resonance wavelength create sensing or detecting ability of the proposed MA with an excellent linear alteration.

J. COMPARATIVE STUDY

An in-depth comparative study with previous works on nanostructured metamaterial absorbers has been illustrated in Table 2. There has been a consideration for the parameters of the PMA, for example, the number of peaks, structural dimension, the wavelength range, the absorption percentage.

A PMA covering the entire optical range is preferable, as discussed earlier. First, the construction of this proposed design consisted of an ultra-thin and small-sized material with a temperature stable far higher than most other materials.

TABLE 2. Comparison between previous works with the proposed design.

Authors	Ustunsoy et al. [41]	Yu et al. [45]	Zhang et al. [46]	Hossain et al. [48]	Qin et al. [49]	Yingying et al. [50]	Chen et al. [79]	Pinghui et al. [81]	Proposed Design
Materials Used	Al, GaAs	Ti, SiO_2	Al, SiO_2	Al, GaAs	Au, SiO_2	Cu, SiO_2	Au, Glass	Au, SiO_2	Al, GaAs
Design Structure	Square shape	Symmetric shape	Rectangular Shape	Circular Shape	Cuboid array shape	Split ring arrays	vertical-square-split-ring (VSSR)	Metal rings shape	Octagonal shape
Absorption Peaks	2	3	2	3	3	3	2	3	4
Dimension	500 × 500 nm^2	500 × 500 nm^2	370 × 370 nm^2	690.52 × 690.52 nm^2	600 × 600 nm^2	800 × 800 × 300 nm^3	500 × 500 × 600 nm^3	1000×1000× 530 nm^3	566 × 566 × 410 nm^3
Range	0 – 600THz	200 – 1900nm	400 – 700nm	200 – 700THz	1000 – 2500nm	800-1500nm	150-550THz		400 – 700nm
Rate of Absorption in Different Peaks with wavelength	99.99% at 568.75 THz, 99% at 216.8 THz	96.67% at 538.9 nm, 98.63% at 954.2 nm, 98.20% at 1726.5 nm	Above 95% at 450 nm and 584 nm	99.74% at 245.03 THz, 99.23% at 376.13 THz, 99.82% at 502.1 THz	96.8% at 1115 nm, 99.6% at 1593 nm, 9.2% at 2039 nm	87.1% at 872.54nm, 99.9% at 1008.69nm, 99.6% at 1138.62nm	99.4% at 239.2 THz, 98.3% at 312.7THz, 99.8% at 476.2THz	96.2% at 459THz, 99.9% at 614THz, 95.8% at 630THz	99.27% at 454.75 nm 99.89% at 505.53 nm, 99.91% at 568.72 nm, 99.06% at 600.85 nm
Polarization Insensitive	Yes	Yes	Not mentioned	Yes	Yes	Yes	Yes	yes	Yes
Angular Stability upto 70% Absorbance	Not mentioned	45˚	Not mentioned	Not mentioned	40˚	60˚	Not mentioned	60˚	60˚
Year	2016	2020	2018	2019	2020	2020	2019	2020	2021

Since the suggested MA is to be operating in the sunlight, it is essential to achieve high-temperature stability. Also, the design of the resonator is very simple and can be fabricated in a simple way rather than other designs discussed below. Secondly, in this proposed design relatively more acquirable materials have been used rather than other materials like gold, titanium, silicon dioxide, copper, etc. Third, an important superiority of this design is that the design is wide angular stable which is a key feature for implementation in solar energy harvesting applications and solar sensors. Another important aspect is that the proposed design is not using quarts or glass as dielectric substances because it uses aluminum as a ground layer. This functionality would also reduce the expense of this design very efficiently. Moreover, this proposed PMA is a remarkable choice for many optical wavelength applications with four high absorption peaks above 99%, and the other characteristics described above.

IV. CONCLUSION

For the inspection of absorbance and other characteristics of an MA with the numerical analysis, a polarization-insensitive incident angular stable octagonal-shaped PMA design was proposed here with Al and GaAs. The proposed design was very simple, ultrathin, and basic, and it has a peak of 99.91% absorbance at the visible regime with four peaks above 99%. Thus, by impedance matching metal with loss-free and lower refractive index dielectric substance, PMA having high absorptivity can be solicitude with necessary behaviors like polarization independency and incident angular independence in both TE and TM modes. In addition, to understand and visualize the absorptivity properly, the e-field, h-field, and surface current distribution are displayed and inspected intensively. Moreover, high inductive and capacitive coupling between resonator and ground layer guarantee outstanding confinement of the EM wave. As the optical wavelength is highly demandable, the suggested MA is perfect for STPV systems, solar sensors, light trapping, light modulator, or light detector applications. Excellent glucose concentration sensing characteristics were also demonstrated. This proposed design structure is quite simple and flexible so that it can be easily possible for industrial implementation with multi-band operations. Also, the related investigation was conducted based on absorption peaks, dimension, and rate of absorption, etc. The enhanced efficiency of these PMAs, as well as their many possible uses, open up new opportunities in the optical wavelength continuum.

AUTHORS CONTRIBUTIONS

Conceptualization, Sultan Mahmud, Minhazul Karim, Sikder Sunbeam Islam, and Mohammad T. Islam; Data curation, Sultan Mahmud, Minhazul Karim, Md Mizan Kabir Shuvo, Tanzina Akter; Formal analysis, Sultan Mahmud, Minhazul Karim, Sikder Sunbeam Islam; Funding acquisition, Ali F. Almutairi and Mohammad T. Islam; Investigation, Sultan Mahmud, Sikder Sunbeam Islam, Tanzina Akter; Methodology, Minhazul Karim, Sikder Sunbeam Islam, Md Mizan Kabir Shuvo; Software and Resources, Ali F. Almutairi and Mohammad T. Islam; Supervision, Mohammad T. Islam; Visualization, Sultan Mahmud, Sikder Sunbeam Islam, Ali F. Almutairi and Mohammad T. Islam; Writing – original draft, Sultan Mahmud, Minhazul Karim, Md Mizan Kabir Shuvo, Tanzina Akter; Writing–review & editing, Sikder Sunbeam Islam, Ali F. Almutairi and Mohammad T. Islam.

REFERENCES

[1] A. Dan, H. C. Barshilia, K. Chattopadhyay, and B. Basu, "Solar energy absorption mediated by surface plasma polaritons in spectrally selective dielectric-metal-dielectric coatings: A critical review," *Renew. Sustain. Energy Rev.*, vol. 79, pp. 1050–1077, Nov. 2017, doi: 10.1016/j.rser.2017.05.062.

[2] Z. Chen, B. Guo, Y. Yang, and C. Cheng, "Metamaterials-based enhanced energy harvesting: A review," *Phys. B, Condens. Matter*, vol. 438, pp. 1–8, Apr. 2014, doi: 10.1016/j.physb.2013.12.040.

[3] Z. Yi, J. Li, J. Lin, F. Qin, X. Chen, W. Yao, Z. Liu, S. Cheng, P. Wu, and H. Li, "Broadband polarization-insensitive and wide-angle solar energy absorber based on tungsten ring-disc array," *Nanoscale*, vol. 12, no. 45, pp. 23077–23083, Nov. 2020, doi: 10.1039/d0nr04502k.

[4] F. Qin, X. Chen, Z. Yi, W. Yao, H. Yang, Y. Tang, Y. Yi, H. Li, and Y. Yi, "Ultra-broadband and wide-angle perfect solar absorber based on TiN nanodisk and Ti thin film structure," *Sol. Energy Mater. Sol. Cells*, vol. 211, Jul. 2020, Art. no. 110535, doi: 10.1016/j.solmat.2020.110535.

[5] R. Jadeja, S. Charola, S. K. Patel, J. Parmar, M. Ladumor, T. K. Nguyen, and V. Dhasarathan, "Numerical investigation of graphene-based efficient and broadband metasurface for terahertz solar absorber," *J. Mater. Sci.*, vol. 55, no. 8, pp. 3462–3469, Mar. 2020, doi: 10.1007/s10853-019-04269-y.

[6] C. M. Soukoulis, S. Linden, and M. Wegener, "Negative refractive index at optical wavelengths," *Science*, vol. 315, no. 5808, pp. 47–49, Jan. 2007, doi: 10.1126/science.1136481.

[7] R. W. Ziolkowski, "Design, fabrication, and testing of double negative metamaterials," *IEEE Trans. Antennas Propag.*, vol. 51, no. 7, pp. 1516–1529, Jul. 2003, doi: 10.1109/TAP.2003.813622.

[8] V. G. Veselago, "The electrodynamics of substances with simultaneously negative values of ϵ and μ," *Sov. Phys. Uspekhi*, vol. 10, no. 4, pp. 509–514, Apr. 1968.

[9] D. R. Smith, W. J. Padilla, D. C. Vier, S. C. Nemat-Nasser, and S. Schultz, "Composite medium with simultaneously negative permeability and permittivity," *Phys. Rev. Lett.*, vol. 84, pp. 4184–4187, May 2000, doi: 10.1103/PhysRevLett.84.4184.

[10] S. Hannan, M. T. Islam, A. Hoque, M. J. Singh, and A. F. Almutairi, "Design of a novel double negative metamaterial absorber atom for Ku and K band applications," *Electron.*, vol. 8, no. 8, pp. 1–16, 2019, doi: 10.3390/electronics8080853.

[11] A. Hoque, M. T. Islam, A. F. Almutairi, M. E. H. Chowdhury, and M. Samsuzzaman, "SNG and DNG meta-absorber with fractional absorption band for sensing application," *Sci. Rep.*, vol. 10, no. 1, pp. 1–17, Aug. 2020, doi: 10.1038/s41598-020-69792-4.

[12] Z. Liu, X. Liu, Y. Wang, G. Liu, and C. Tang, "Silicon antennas metasurface based light absorber with quantitatively adjustable operating frequency and intensity," *IEEE J. Sel. Topics Quantum Electron.*, vol. 27, no. 1, pp. 1–6, Jan. 2021, doi: 10.1109/JSTQE.2020.2987179.

[13] N. I. Landy, S. Sajuyigbe, J. J. Mock, D. R. Smith, and W. J. Padilla, "Perfect metamaterial absorber," *Phys. Rev. Lett.*, vol. 100, no. 20, May 2008, Art. no. 207402, doi: 10.1103/PhysRevLett.100.207402.

[14] H. Zou and Y. Cheng, "Design of a six-band terahertz metamaterial absorber for temperature sensing application," *Opt. Mater.*, vol. 88, pp. 674–679, Feb. 2019, doi: 10.1016/j.optmat.2019.01.002.

[15] Y. Cheng, X. S. Mao, C. Wu, L. Wu, and R. Z. Gong, "Infrared non-planar plasmonic perfect absorber for enhanced sensitive refractive index sensing," *Opt. Mater.*, vol. 53, pp. 195–200, Mar. 2016, doi: 10.1016/j.optmat.2016.01.053.

[16] H. Luo and Y. Z. Cheng, "Design of an ultrabroadband visible metamaterial absorber based on three-dimensional metallic nanostructures," *Modern Phys. Lett. B*, vol. 31, no. 25, Sep. 2017, Art. no. 1750231, doi: 10.1142/S0217984917502311.

[17] S. Mahmud, S. S. Islam, A. F. Almutairi, and M. T. Islam, "A wide incident angle, ultrathin, polarization-insensitive metamaterial absorber for optical wavelength applications," *IEEE Access*, vol. 8, pp. 129525–129541, 2020, doi: 10.1109/ACCESS.2020.3008429.

[18] J. Wang, Y. Chen, J. Hao, M. Yan, and M. Qiu, "Shape-dependent absorption characteristics of three-layered metamaterial absorbers at near-infrared," *J. Appl. Phys.*, vol. 109, no. 7, Apr. 2011, Art. no. 074510, doi: 10.1063/1.3573495.

[19] Y.-C. Lai, C.-Y. Chen, Y.-T. Hung, and C.-Y. Chen, "Extending absorption edge through the hybrid resonator-based absorber with wideband and near-perfect absorption in visible region," *Materials*, vol. 13, no. 6, p. 1470, Mar. 2020, doi: 10.3390/ma13061470.

[20] K. Aydin, V. E. Ferry, R. M. Briggs, and H. A. Atwater, "Broadband polarization-independent resonant light absorption using ultrathin plasmonic super absorbers," *Nature Commun.*, vol. 2, no. 517, pp. 1–7, Nov. 2011, doi: 10.1038/ncomms1528.

[21] N. Mattiucci, M. J. Bloemer, N. Aközbek, and G. D'Aguanno, "Impedance matched thin metamaterials make metals absorbing," *Sci. Rep.*, vol. 3, no. 1, pp. 1–11, Dec. 2013, doi: 10.1038/srep03203.

[22] R. Contractor, G. D'Aguanno, and C. Menyuk, "Ultra-broadband, polarization-independent, wide-angle absorption in impedance-matched metamaterials with anti-reflective moth-eye surfaces," *Opt. Exp.*, vol. 26, no. 18, Sep. 2018, Art. no. 24031, doi: 10.1364/oe.26.024031.

[23] T. S. Tuan and N. T. Q. Hoa, "Numerical study of an efficient broadband metamaterial absorber in visible light region," *IEEE Photon. J.*, vol. 11, no. 3, pp. 1–10, Jun. 2019, doi: 10.1109/JPHOT.2019.2910806.

[24] D. Katrodiya, C. Jani, V. Sorathiya, and S. K. Patel, "Metasurface based broadband solar absorber," *Opt. Mater.*, vol. 89, pp. 34–41, Mar. 2019, doi: 10.1016/j.optmat.2018.12.057.

[25] S. Lee, T. Q. Tran, H. Heo, M. Kim, and S. Kim, "A proposal of a perfect graphene absorber with enhanced design and fabrication tolerance," *Sci. Rep.*, vol. 7, no. 1, pp. 1–10, Dec. 2017, doi: 10.1038/s41598-017-04995-w.

[26] X. Han, K. He, Z. He, and Z. Zhang, "Tungsten-based highly selective solar absorber using simple nanodisk array," *Opt. Exp.*, vol. 25, no. 24, Nov. 2017, Art. no. A1072, doi: 10.1364/oe.25.0a1072.

[27] S. Mahmud, S. S. Islam, K. Mat, M. E. H. Chowdhury, H. Rmili, and M. T. Islam, "Design and parametric analysis of a wide-angle polarization-insensitive metamaterial absorber with a star shape resonator for optical wavelength applications," *Results Phys.*, vol. 18, Sep. 2020, Art. no. 103259, doi: 10.1016/j.rinp.2020.103259.

[28] M. J. Hossain, M. R. I. Faruque, and M. T. Islam, "Perfect metamaterial absorber with high fractional bandwidth for solar energy harvesting," *PLoS ONE*, vol. 13, no. 11, pp. 1–15, 2018, doi: 10.1371/journal.pone.0207314.

[29] C. Li, H. Fan, Q. Dai, Z. Wei, S. Lan, and H. Liu, "Multipole resonance in arrays of diamond dielectric: A metamaterial perfect absorber in the visible regime," *Nanomaterials*, vol. 9, no. 9, p. 1222, Aug. 2019, doi: 10.3390/nano9091222.

[30] X.-J. He, S.-T. Yan, Q.-X. Ma, Q.-F. Zhang, P. Jia, F.-M. Wu, and J.-X. Jiang, "Broadband and polarization-insensitive terahertz absorber based on multilayer metamaterials," *Opt. Commun.*, vol. 340, pp. 44–49, Apr. 2015, doi: 10.1016/j.optcom.2014.11.068.

[31] Y. Matsuno and A. Sakurai, "Perfect infrared absorber and emitter based on a large-area metasurface," *Opt. Mater. Exp.*, vol. 7, no. 2, p. 618, Feb. 2017, doi: 10.1364/ome.7.000618.

[32] H. Xiong, J.-S. Hong, C.-M. Luo, and L.-L. Zhong, "An ultrathin and broadband metamaterial absorber using multi-layer structures," *J. Appl. Phys.*, vol. 114, no. 6, Aug. 2013, Art. no. 064109, doi: 10.1063/1.4818318.

[33] H. Lin, B. C. Sturmberg, K. T. Lin, Y. Yang, X. Zheng, T. K. Chong, C. M. de Sterke, and B. Jia, "A 90-nm-thick graphene metamaterial for strong and extremely broadband absorption of unpolarized light," *Nature Photon.*, vol. 13, pp. 270–276, Mar. 2019, doi: 10.1038/s41566-019-0389-3.

[34] N. T. Q. Hoa, P. D. Tung, P. H. Lam, N. D. Dung, and N. H. Quang, "Numerical study of an ultrabroadband, wide-angle, polarization-insensitivity metamaterial absorber in the visible region," *J. Electron. Mater.*, vol. 47, no. 5, pp. 2634–2639, May 2018, doi: 10.1007/s11664-018-6100-5.

[35] A. Selamat, N. Misran, M. F. Mansor, M. T. Islam, and S. H. Zaidi, "Scattering microwave signal analysis from triangular loop element of different transparent conductive thin films at Ku-band," *Jurnal Kejuruteraan*, vol. 26, pp. 83–88, Dec. 2014.

[36] S. Wu, Y. Ye, Z. Jiang, T. Yang, and L. Chen, "Large-area, ultrathin metasurface exhibiting strong unpolarized ultrabroadband absorption," *Adv. Opt. Mater.*, vol. 7, no. 24, pp. 1–7, 2019, doi: 10.1002/adom.201901162.

[37] A. Ghobadi, H. Hajian, M. Gokbayrak, B. Butun, and E. Ozbay, "Bismuth-based metamaterials: From narrowband reflective color filter to extremely broadband near perfect absorber," *Nanophotonics*, vol. 8, no. 5, pp. 823–832, Mar. 2019, doi: 10.1515/nanoph-2018-0217.

[38] S. Hannan, M. T. Islam, A. F. Almutairi, and M. R. I. Faruque, "Wide bandwidth angle- and polarization-insensitive symmetric metamaterial absorber for X and Ku band applications," *Sci. Rep.*, vol. 10, no. 1, pp. 1–9, Dec. 2020, doi: 10.1038/s41598-020-67262-5.

[39] J. Liu, M. Zhu, N. Zhang, H. Zhang, Y. Zhou, S. Sun, N. Yi, S. Gao, Q. Song, and S. Xiao, "Wafer-scale metamaterials for polarization-insensitive and dual-band perfect absorption," *Nanoscale*, vol. 7, no. 45, pp. 18914–18917, 2015, doi: 10.1039/c5nr05479f.

[40] A. M. Montaser, "Design of metamaterial absorber for all bands from microwave to terahertz ranges," *J. Adv. Res. Electron. Commun. Eng.*, vol. 5, no. 5, pp. 1475–1481, 2016.

[41] M. P. Ustunsoy and C. Sabah, "Dual-band high-frequency metamaterial absorber based on patch resonator for solar cell applications and its enhancement with graphene layers," *J. Alloys Compounds*, vol. 687, pp. 514–520, Dec. 2016, doi: 10.1016/j.jallcom.2016.06.143.

[42] B. Mulla and C. Sabah, "Multiband metamaterial absorber design based on plasmonic resonances for solar energy harvesting," *Plasmonics*, vol. 11, no. 5, pp. 1313–1321, Oct. 2016, doi: 10.1007/s11468-015-0177-y.

[43] M. K. Hedayati, M. Javaherirahim, B. Mozooni, R. Abdelaziz, A. Tavassolizadeh, V. S. K. Chakravadhanula, V. Zaporojtchenko, T. Strunkus, F. Faupel, and M. Elbahri, "Design of a perfect black absorber at visible frequencies using plasmonic metamaterials," *Adv. Mater.*, vol. 23, no. 45, pp. 5410–5414, Dec. 2011, doi: 10.1002/adma.201102646.

[44] T. Cao, C.-W. Wei, R. E. Simpson, L. Zhang, and M. J. Cryan, "Broadband polarization-independent perfect absorber using a phase-change metamaterial at visible frequencies," *Sci. Rep.*, vol. 4, no. 1, pp. 1–8, May 2015, doi: 10.1038/srep03955.

[45] P. Yu, H. Yang, X. Chen, Z. Yi, W. Yao, J. Chen, Y. Yi, and P. Wu, "Ultra-wideband solar absorber based on refractory titanium metal," *Renew. Energy*, vol. 158, pp. 227–235, Oct. 2020, doi: 10.1016/j.renene.2020.05.142.

[46] Z. Zhang, Z. Yu, Y. Liang, and T. Xu, "Dual-band nearly perfect absorber at visible frequencies," *Opt. Mater. Exp.*, vol. 8, no. 2, p. 463, Feb. 2018, doi: 10.1364/ome.8.000463.

[47] Q. Mao, C. Feng, and Y. Yang, "Design of tunable multi-band metamaterial perfect absorbers based on magnetic polaritons," *Plasmonics*, vol. 14, no. 2, pp. 389–396, Apr. 2019, doi: 10.1007/s11468-018-0816-1.

[48] M. J. Hossain, M. R. I. Faruque, M. R. Ahmed, M. J. Alam, and M. T. Islam, "Polarization-insensitive infrared-visible perfect metamaterial absorber and permittivity sensor," *Results Phys.*, vol. 14, Sep. 2019, Art. no. 102429, doi: 10.1016/j.rinp.2019.102429.

[49] F. Qin, Z. Chen, X. Chen, Z. Yi, W. Yao, T. Duan, P. Wu, H. Yang, G. Li, and Y. Yi, "A tunable triple-band near-infrared metamaterial absorber based on Au nano-cuboids array," *Nanomaterials*, vol. 10, no. 2, p. 207, Jan. 2020, doi: 10.3390/nano10020207.

[50] Y. Wang, Z. Chen, D. Xu, Z. Yi, X. Chen, J. Chen, Y. Tang, P. Wu, G. Li, and Y. Yi, "Triple-band perfect metamaterial absorber with good operating angle polarization tolerance based on split ring arrays," *Results Phys.*, vol. 16, Mar. 2020, Art. no. 102951, doi: 10.1016/j.rinp.2020.102951.

[51] Z. Li, C. Luo, G. Yao, J. Yue, J. Ji, J. Yao, and F. Ling, "Design of a concise and dual-band tunable metamaterial absorber," *Chin. Opt. Lett.*, vol. 14, no. 10, Oct. 2016, Art. no. 102303.

[52] M. Bağmancı, M. Karaaslan, E. Ünal, O. Akgol, F. Karadağ, and C. Sabah, "Broad-band polarization-independent metamaterial absorber for solar energy harvesting applications," *Phys. E, Low-Dimensional Syst. Nanostruct.*, vol. 90, pp. 1–6, Jun. 2017, doi: 10.1016/j.physe.2017.03.001.

[53] E. Shiles, T. Sasaki, M. Inokuti, and D. Y. Smith, "Self-consistency and sum-rule tests in the Kramers-Kronig analysis of optical data: Applications to aluminum," *Phys. Rev. B, Condens. Matter*, vol. 22, no. 4, pp. 1612–1628, Aug. 1980, doi: 10.1103/PhysRevB.22.1612.

[54] V. E. Ferry, L. A. Sweatlock, D. Pacifici, and H. A. Atwater, "Plasmonic nanostructure design for efficient light coupling into solar cells," *Nano Lett.*, vol. 8, no. 12, pp. 4391–4397, Dec. 2008, doi: 10.1021/nl8022548.

[55] E. D. Kosten, J. H. Atwater, J. Parsons, A. Polman, and H. A. Atwater, "Highly efficient GaAs solar cells by limiting light emission angle," *Light, Sci. Appl.*, vol. 2, no. 1, p. e45, Jan. 2013, doi: 10.1038/lsa.2013.1.

[56] R. Y. Loo, G. S. Kamath, and S. S. Li, "Radiation damage and annealing in GaAs solar cells," *IEEE Trans. Electron Devices*, vol. 37, no. 2, pp. 485–497, Feb. 1990, doi: 10.1109/16.46387.

[57] D. R. Smith, D. C. Vier, T. Koschny, and C. M. Soukoulis, "Electromagnetic parameter retrieval from inhomogeneous metamaterials," *Phys. Rev. E, Stat. Phys. Plasmas Fluids Relat. Interdiscip. Top.*, vol. 71, no. 3, pp. 1–11, Mar. 2005, doi: 10.1103/PhysRevE.71.036617.

[58] E. J. Rothwell, J. L. Frasch, S. M. Ellison, P. Chahal, and R. O. Ouedraogo, "Analysis of the nicolson-ross-weir method for characterizing the electromagnetic properties of engineered materials," *Prog. Electromagn. Res.*, vol. 157, pp. 31–47, 2016, doi: 10.2528/PIER16071706.

[59] D. Y. Smit, E. Shiles, and M. Inokuti, *The Optical Properties of Metallic Aluminum**Work Supported by the U.S. Department of Energy*, S. Palik, Ed. Boston, MA, USA: Academic, 1985, pp. 369–406.

[60] S. M. Choudhury, D. Wang, K. Chaudhuri, C. DeVault, A. V. Kildishev, A. Boltasseva, and V. M. Shalaev, "Material platforms for optical metasurfaces," *Nanophotonics*, vol. 7, no. 6, pp. 959–987, Jun. 2018, doi: 10.1515/nanoph-2017-0130.

[61] A. Hoque, M. T. Islam, A. F. Almutairi, and M. R. I. Faruque, "Design of split hexagonal patch array shaped nano-metaabsorber with ultra-wideband absorption for visible and UV spectrum application," *Nanosc. Res. Lett.*, vol. 14, no. 1, pp. 1–10, Dec. 2019, doi: 10.1186/s11671-019-3231-4.

[62] A. Hoque, M. T. Islam, A. Almutairi, T. Alam, M. J. Singh, and N. Amin, "A polarization independent quasi-TEM metamaterial absorber for X and Ku band sensing applications," *Sensors*, vol. 18, no. 12, p. 4209, Nov. 2018, doi: 10.3390/s18124209.

[63] J. K. Kitur, L. Gu, T. Tumkur, C. Bonner, and M. A. Noginov, "Stimulated emission of surface plasmons on top of metamaterials with hyperbolic dispersion," *ACS Photon.*, vol. 2, no. 8, pp. 1019–1024, Aug. 2015, doi: 10.1021/ph500475x.

[64] P. Zhu and L. Jay Guo, "High performance broadband absorber in the visible band by engineered dispersion and geometry of a metal-dielectric-metal stack," *Appl. Phys. Lett.*, vol. 101, no. 24, Dec. 2012, Art. no. 241116, doi: 10.1063/1.4771994.

[65] Q. Feng, M. Pu, C. Hu, and X. Luo, "Engineering the dispersion of metamaterial surface for broadband infrared absorption," *Opt. Lett.*, vol. 37, no. 11, p. 2133, Jun. 2012, doi: 10.1364/ol.37.002133.

[66] Y. Jin, J. Park, Y. Rah, J. Shim, and K. Yu, "Ultrahigh omnidirectional, broadband, and polarization-independent optical absorption over the visible wavelengths by effective dispersion engineering," *Sci. Rep.*, vol. 9, no. 1, pp. 1–10, Dec. 2019, doi: 10.1038/s41598-019-46413-3.

[67] H. M. Lee and J. C. Wu, "A wide-angle dual-band infrared perfect absorber based on metal–dielectric–metal split square-ring and square array," *J. Phys. D, Appl. Phys.*, vol. 45, no. 20, May 2012, Art. no. 205101, doi: 10.1088/0022-3727/45/20/205101.

[68] S. Cao, W. Yu, T. Wang, Z. Xu, C. Wang, Y. Fu, and Y. Liu, "Two-dimensional subwavelength meta-nanopillar array for efficient visible light absorption," *Appl. Phys. Lett.*, vol. 102, no. 16, pp. 1–5, 2013, doi: 10.1063/1.4803046.

[69] N. Liu, H. Guo, L. Fu, S. Kaiser, H. Schweizer, and H. Giessen, "Three-dimensional photonic metamaterials at optical frequencies," *Nature Mater.*, vol. 7, no. 1, pp. 31–37, 2008, doi: 10.1038/nmat2072.

[70] H.-T. Chen, "Interference theory of metamaterial perfect absorbers," *Opt. Exp.*, vol. 20, no. 7, p. 7165, Mar. 2012, doi: 10.1364/oe.20.007165.

[71] T. Wanghuang, W. Chen, Y. Huang, and G. Wen, "Analysis of metamaterial absorber in normal and oblique incidence by using interference theory," *AIP Adv.*, vol. 3, no. 10, Oct. 2013, Art. no. 102118, doi: 10.1063/1.4826522.

[72] F. Dincer, M. Karaaslan, E. Unal, O. Akgol, and C. Sabah, "Design of polarization- and incident angle-independent perfect metamaterial absorber with interference theory," *J. Electron. Mater.*, vol. 43, no. 11, pp. 3949–3953, Nov. 2014, doi: 10.1007/s11664-014-3316-x.

[73] S. Quader, M. R. Akram, F. Xiao, and W. Zhu, "Graphene based ultra-broadband terahertz metamaterial absorber with dual-band tunability," *J. Opt.*, vol. 22, no. 9, Sep. 2020, Art. no. 095104, doi: 10.1088/2040-8986/aba814.

[74] K. Wu, Y. Huang, T. Wanghuang, W. Chen, and G. Wen, "Numerical and theoretical analysis on the absorption properties of metasurface-based terahertz absorbers with different thicknesses," *Appl. Opt.*, vol. 54, no. 2, p. 299, Jan. 2015, doi: 10.1364/ao.54.000299.

[75] C. Liu, L. Qi, and M. Wu, "Triple-broadband infrared metamaterial absorber with polarization-independent and wide-angle absorption," *Opt. Mater. Exp.*, vol. 8, no. 8, p. 2439, Aug. 2018, doi: 10.1364/ome.8.002439.

[76] S. K. Chamoli, S. C. Singh, and C. Guo, "Design of extremely sensitive refractive index sensors in infrared for blood glucose detection," *IEEE Sensors J.*, vol. 20, no. 9, pp. 4628–4634, May 2020, doi: 10.1109/JSEN.2020.2964715.

[77] E. D. Palik, *Handbook of Optical Constants of Solids II*, vol. 1, no. 1. Boston, MA, USA: Academic, 1991, pp. 77–135.

[78] J. Xu, Z. Zhao, H. Yu, L. Yang, P. Gou, J. Cao, Y. Zou, J. Qian, T. Shi, Q. Ren, and Z. An, "Design of triple-band metamaterial absorbers with refractive index sensitivity at infrared frequencies," *Opt. Exp.*, vol. 24, no. 22, Oct. 2016, Art. no. 25742, doi: 10.1364/oe.24.025742.

[79] Y. Cheng, H. Luo, F. Chen, and R. Gong, "Triple narrow-band plasmonic perfect absorber for refractive index sensing applications of optical frequency," *OSA Continuum*, vol. 2, no. 7, p. 2113, Jul. 2019, doi: 10.1364/osac.2.002113.
[80] S. K. Patel, J. Parmar, H. Trivedi, R. Zakaria, T. K. Nguyen, and V. Dhasarathan, "Highly sensitive graphene-based refractive index biosensor using gold metasurface array," *IEEE Photon. Technol. Lett.*, vol. 32, no. 12, pp. 681–684, Jun. 15, 2020, doi: 10.1109/LPT.2020.2992085.
[81] P. Wu, C. Zhang, Y. Tang, B. Liu, and L. Lv, "A perfect absorber based on similar Fabry-Pérot four-band in the visible range," *Nanomaterials*, vol. 10, no. 3, pp. 1–10, 2020, doi: 10.3390/nano10030488.

SULTAN MAHMUD received the B.Sc. degree from the Department of Electrical and Electronic Engineering, International Islamic University Chittagong (IIUC), Bangladesh, in 2020.

He completed his undergraduate thesis on metamaterial-based absorbers for optical wavelength applications. He is currently working on some metamaterial absorbers in the optical and microwave range. His main research interests include metamaterials, metamaterial absorbers for optical, and microwave applications. He has been serving as a Reviewer for IEEE Access.

MINHAZUL KARIM received the B.Sc. degree from the Department of Electrical and Electronic Engineering, International Islamic University Chittagong, Bangladesh, in 2021. He completed his undergraduate thesis on metamaterial absorbers for solar thermo-photovoltaic (STPV) systems. His research interests include metamaterials and metamaterial-based absorbers for solar applications.

SIKDER SUNBEAM ISLAM (Member, IEEE) received the B.Sc. degree in electrical and electronic engineering in Bangladesh, in 2005, the M.Sc. degree in mobile computing and communications from the University of Greenwich, U.K., in 2008, the Ph.D. degree in space science from the National University of Malaysia, Malaysia, in 2017.

He is currently an Associate Professor and the Department Head with the Department of Electrical and Electronic Engineering, International Islamic University Chittagong, Bangladesh. He has one published book and many publications in international proceedings and journals. His main research interests include metamaterial for communications, electromagnetic radiation, and mobile computing.

Dr. Islam has been serving as a reviewer for several international conferences and journals.

MD MIZAN KABIR SHUVO received the B.Sc. degree from the Department of Electrical and Electronic Engineering, Mymensingh Engineering College, University of Dhaka, Bangladesh, in 2021. His undergraduate thesis was on a metamaterial-based broadband absorber for the optical regime, which he completed. His main research interests include metamaterial absorber, MRR, and the IoT-based systems.

TANZINA AKTER is currently pursuing the bachelor's degree with the Department of Chemistry, Government City College Chittagong under the National University, Bangladesh.

She is currently working on some metamaterial absorber-based research work. She wants to build up her research career in biomedical engineering. Her main research interests include metamaterials and metamaterial absorbers for biomedical and optical applications.

ALI F. ALMUTAIRI (Senior Member, IEEE) received the B.S. degree in electrical engineering from the University of South Florida, Tampa, FL, USA, in 1993, and the M.S. and Ph.D. degrees in electrical engineering from the University of Florida, Gainesville, FL, USA, in 1995 and 2000, respectively. He served as the Chairperson for the Electrical Engineering Department, Kuwait University, from March 2007 to September 2011, and served as the Graduate Program Director for the Electrical Engineering Department, Kuwait University, from September 2015 to September 2016. He served as the Vice Dean for academic affairs at the College of Engineering and Petroleum, Kuwait University, from March 2016 to July 2018. He was the Dean of admission and registration at Kuwait University, from July 2018 to December 2020. At the present, he is currently a Professor with the Electrical Engineering Department. His current research interests include multiuser detection, wireless networks, antenna design, and current and future cellular networks performance issues. He is a member of other professional societies. In December 1993, he has been awarded a Full Scholarship from Kuwait University to pursue his graduate studies. He served/serving as an associate editor and a reviewer for many technical publications.

MOHAMMAD TARIQUL ISLAM (Senior Member, IEEE) is currently a Professor with the Department of Electrical, Electronic and Systems Engineering, Universiti Kebangsaan Malaysia (UKM), and a Visiting Professor with the Kyushu Institute of Technology, Japan. He is an author and coauthor of about 500 research journal articles, nearly 200 conference articles, and a few book chapters on various topics related to antennas, metamaterials, and microwave imaging with 22 inventory patents filed. Thus far, his publications have been cited 7300 times and his H-index is 41 (Source: Scopus). His Google scholar citation is 11,850 and his H-index is 49. He has supervised about 30 Ph.D. theses, 20 M.Sc. theses, and has mentored more than ten postdoctoral and visiting scholars. He has developed the Antenna Measurement Laboratory which includes antenna design and measurement facility till 40 GHz. His research interests include communication antenna design, metamaterial, satellite antennas, and microwave imaging. He has been serving as an Executive Committee Member for IEEE AP/MTT/EMC Malaysia Chapter, from 2019 to 2020, the Chartered Professional Engineer (CEng), a fellow of IET, U.K., and a Senior Member of IEICE, Japan. He was a recipient of more than 40 research grants from the Malaysian Ministry of Science, Technology and Innovation, Ministry of Education, UKM research grant, international research grants from Japan, Saudi Arabia, and Kuwait. He received several International Gold Medal Award, the Best Invention in Telecommunication Award for his Research and Innovation, and the Best Researcher Awards at UKM. He was a recipient of the 2018, 2019, and 2020 IEEE AP/MTT/EMC Malaysia Chapter, Excellent Award. He also won the Best Innovation Award and the Best Research Group in ICT Niche by UKM, in different years. He was a recipient of the Publication Award from the Malaysian Space Agency, in several years. He was an Associate Editor of *IET Electronics Letter*. He also serves as the Guest Editor for *Sensors journal* and an Associate Editor for IEEE Access.